STRUCTURAL BIOLOGY

ISSN 2059-7983

Phosphoramidon inhibits the integral membrane protein zinc metalloprotease ZMPSTE24

Brandon R. Goblirsch, Buenafe T. Arachea,‡ Daniel J. Councell and Michael C. Wiener*

Department of Molecular Physiology and Biological Physics, University of Virginia, Charlottesville, VA 22908-0886, USA. *Correspondence e-mail: mwiener@virginia.edu

Received 7 November 2017
Accepted 27 February 2018

Edited by P. Langan, Oak Ridge National Laboratory, USA

‡ Current address: Merck & Co., Elkton, VA 22827, USA.

Keywords: phosphoramidon; ZMPSTE24; zinc metalloprotease.

PDB reference: ZMPSTE24 in complex with phosphoramidon, 6bh8

Supporting information: this article has supporting information at journals.iucr.org/d

The integral membrane protein zinc metalloprotease ZMPSTE24 possesses a completely novel structure, comprising seven long kinked transmembrane helices that encircle a voluminous 14 000 Å^3 cavity within the membrane. Functionally conserved soluble zinc metalloprotease residues are contained within this cavity. As part of an effort to understand the structural and functional relationships between ZMPSTE24 and soluble zinc metalloproteases, the inhibition of ZMPSTE24 by phosphoramidon [*N*-(α-rhamnopyranosyl-oxy-hydroxyphosphinyl)-Leu-Trp], a transition-state analog and competitive inhibitor of multiple soluble zinc metalloproteases, especially gluzincins, has been characterized functionally and structurally. The functional results, the determination of preliminary IC_{50} values by the use of an intramolecular quenched-fluorescence fluorogenic peptide assay, indicate that phosphoramidon inhibits ZMPSTE24 in a manner consistent with competitive inhibition. The structural results, a 3.85 Å resolution X-ray crystal structure of a ZMPSTE24–phosphoramidon complex, indicate that the overall binding mode observed between phosphoramidon and soluble gluzincins is conserved. Based on the structural data, a significantly lower potency than that observed for soluble gluzincins such as thermolysin and neprilysin is predicted. These results strongly suggest a close relationship between soluble gluzincins and the integral membrane protein zinc metalloprotease ZMPSTE24.

1. Introduction

Proteases are abundant, with the mammalian degradome containing approximately 2% of genome-encoded proteins (Ordóñez *et al.*, 2009). Proteases are found in virtually every cell and tissue type, and conduct a remarkably broad range of biological functions. The human zinc metalloprotease ZMPSTE24, localized to the endoplasmic reticulum (ER) and inner nuclear membranes (Barrowman *et al.*, 2008), processes prelamin A, the precursor of the nuclear intermediate filament protein lamin A. Lamins comprise nuclear lamina, which provide mechanical stability to the nuclear envelope and function as scaffolds for DNA repair and replication complexes (Dittmer & Misteli, 2011). Mutations in either ZMPSTE24 or prelamin A are associated with a spectrum of accelerated-aging diseases referred to as progerias (Worman, 2012), and the severity of different progerias appears to be correlated with the extent of loss of ZMPSTE24 activity (Barrowman *et al.*, 2012). Because of its role in progerias, ZMPSTE24 has also been investigated as a biomarker for vascular aging (Ragnauth *et al.*, 2010). Additionally, lipodystrophy acquired from antiretroviral therapy used to treat AIDS patients is likely to result from off-target interactions of HIV (aspartyl) protease-inhibitor drugs with ZMPSTE24

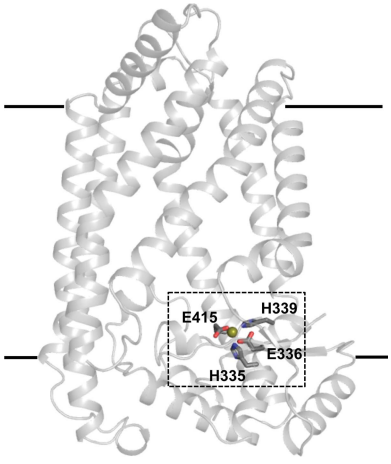

(Coffinier *et al.*, 2007; Goulbourne & Vaux, 2010). Historically, ZMPSTE24 has been classified as a 'CaaX protease', recognizing C-terminal tetrapeptide motifs consisting of prenylated (farnesylated or geranylgeranylated) cysteine–aliphatic–aliphatic–anything and cleaving the terminal 'aaX' residues. A series of publications have suggested more general roles for ZMPSTE24 in multiple ER processes, including the proper orientation of a single-pass transmembrane α-helical protein (Tipper & Harley, 2002), the unfolded protein response, a cellular stress response of the ER (Jonikas *et al.*, 2009), and the removal of misfolded proteins that 'clog' the translocon during signal recognition particle (SRP)-independent protein translocation (Ast *et al.*, 2016). A very recent paper (Kayatekin *et al.*, 2018) identified ZMPSTE24 as protecting against human islet amyloid polypeptide oligomer-induced proteotoxicity. A yeast ortholog of ZMPSTE24 has also been implicated in chitin biosynthesis (Meissner *et al.*, 2010). Moreover, a collaborative publication from our group demonstrated that substrate prenylation is dispensable for cleavage by a yeast ortholog of ZMPSTE24 (Hildebrandt *et al.*, 2016).

The first ZMPSTE24 family member to be discovered and characterized was a yeast ortholog which processes a-factor, an essential mating pheromone (Boyartchuk *et al.*, 1997; Fujimura-Kamada *et al.*, 1997). Cloning and sequencing of the gene revealed the presence of the characteristic HE*XX*H 'zincin' motif of zinc metalloproteases (Hooper, 1994); moreover, Boyartchuk *et al.* (1997) commented that the protein sequence '...matched a larger consensus sequence characteristic of neutral Zn metalloproteases'. X-ray crystal structures of ZMPSTE24 and a yeast ortholog (the latter determined by our group) revealed a completely novel integral membrane-protein architecture: seven transmembrane α-helices enclosing a 14 000 Å^3 'reaction chamber' within the membrane interior, which contains the enzyme active-site and substrate-binding residues (Pryor *et al.*, 2013; Quigley *et al.*, 2013). Analysis of these structures included comparisons with thermolysin (Pryor *et al.*, 2013; Quigley *et al.*, 2013) and a bacterial M48 peptidase (Quigley *et al.*, 2013), both of which are gluzincins: zinc metalloproteases containing the sequence HE*XX*H...E (Hooper, 1994). We are pursuing, more deeply, an analysis of ZMPSTE24 in the context of gluzincins, with the goal of determining the extent to which this integral membrane protein zinc metalloprotease of novel structure is identical (or similar) to soluble gluzincins. In other words, fundamental 'gluzincin determinants' are encoded within the sequence and structure of ZMPSTE24, but these features are nested within an intramembrane 'reaction chamber' formed by transmembrane α-helices and located within the nonpolar membrane interior. Might these novel 'non-gluzincin' features fundamentally affect the characteristics of ZMPSTE24 and significantly differentiate its behavior from soluble gluzincins? One 'benchmark' characterization of zinc metalloproteases, and gluzincins in particular, is their level of inhibition by known zinc metalloprotease inhibitors. The natural product phosphoramidon [*N*-(α-rhamnopyranosyloxyhydroxyphosphinyl)-Leu-Trp], a peptide-like molecule secreted by *Streptomyces tanashiensis* and first shown to inhibit thermolysin (Suda *et al.*, 1973), is a transition-state analog and competitive inhibitor of multiple soluble zinc metalloproteases, particularly gluzincins (Salvesen & Narbonne, 2001). Therefore, we considered the functional and structural characterization of the interaction of phosphoramidon with ZMPSTE24 to be an important 'foundational' determinant of the relationship between ZMPSTE24 and soluble gluzincins.

2. Materials and methods

2.1. Materials and reagents

The human *ste24* (*zmpste24*) gene (HsCD00075979) was obtained from the DNASU Plasmid Repository (Arizona State University). *N*-Dodecyl maltoside (DDM) and $C_{12}E_7$ were purchased from Inalco Pharmaceuticals and Anatrace, respectively. The fluorogenic peptide substrate Abz-KSKTKSVIK-Dnp was purchased as a lyophilized powder at >98% purity from Anaspec. [Abz (*ortho*-aminobenzoic acid) is located at the N-terminus of Abz-KSKTKSVIK-Dnp. Dnp (2,4-dinitrophenol), which is located in the modified side chain of ε-Dnp-lysine at the C-terminus of Abz-KSKTKSVIK-Dnp, is a non-emitting FRET acceptor, *i.e.* a quencher, for Abz fluorescence.] Phosphoramidon (sodium salt) was acquired from Cayman Chemicals. All other reagents used for this study were of analytical grade.

2.2. Cloning and expression of ZMPSTE24

The *zmpste24* gene was amplified by polymerase chain reaction and inserted into the yeast (*Saccharomyces cerevisiae*) expression vector pSGP47 using an In-Fusion HD Cloning kit (Clontech Laboratories). The pSGP47-*zmpste24* plasmid contains a C-terminal rhinovirus 3C protease site and a decahistidine tag. pSGP47 uses an *ADH2* promoter, inducing protein expression upon glucose depletion in the medium (Clark *et al.*, 2010).

Protein expression was carried out following previously published protocols with some modifications (Pryor *et al.*, 2013). The pSGP47-*zmpste24* plasmid was transformed into *S. cerevisiae* strain BJ5460 (Jones, 1991; ATCC20885) by the lithium acetate–PEG method (Ito *et al.*, 1983). Starter cultures (120 ml) in sterile CSM-Ura medium were incubated for 18 h at 30°C with shaking at 220 rev min^{-1} (to an OD of ~1.8–2.0). 10 ml starter culture was then transferred into a 2.8 l flask containing 1 l sterile CSM-Ura medium and the cultures were allowed to grow at 30°C for 24 h until the OD reached a value of 1.4. A total of 12 flasks of yeast were prepared for this step. After incubation, yeast cultures were spun at 3500*g* for 15 min. The cell pellets were pooled, resuspended in 500 ml sterile YPD medium and used to inoculate 16 l YPD medium. Additional cell growth was carried out in a fermenter for 26 h at 28°C with the addition of oxygen and agitation at 400 rev min^{-1}. The cells were harvested by centrifugation (3500*g*), flash-cooled in liquid nitrogen and stored at −80°C until use. A 16 l fermenter growth yielded ~320 g of cell paste.

2.3. Membrane preparation

BJ5460 cells with overexpressed ZMPSTE24 (∼160 g) were thawed on ice and resuspended, using a hand-held glass homogenizer, in 160 ml lysis buffer [20 m*M* HEPES, 50 m*M* NaCl, 15%(*w*/*v*) glycerol, 2 m*M* $MgCl_2$, 2 m*M* *β*-mercaptoethanol (*β*ME), 100 µ*M* PMSF, 2.5 µg ml^{-1} leupeptin, 100 U benzonase pH 7.5]. The cells were lysed by three passes at 193 MPa through a microfluidizer (MP-110 with an 87 µm interaction chamber; Microfluidics) with a pre-cooled outlet coil immersed in an ice bath. The lysate was spun at 4000*g* (30 min, 4°C), followed by another spin at 30 000*g* (30 min, 4°C) to pellet unbroken cells. The resulting supernatant from this step was spun at 205 000*g* (90 min, 4°C) to isolate the membrane fraction. Membranes (∼25 g) were resuspended, using a hand-held glass homogenizer, in 150 ml membrane buffer (50 m*M* HEPES, 150 m*M* NaCl, 15% glycerol, 2 m*M* *β*ME, 100 µ*M* PMSF, 2.5 µg ml^{-1} leupeptin pH 7.5). Samples were divided into aliquots, snap-frozen in liquid nitrogen and stored at −80°C until used for purification and enzymatic assays.

2.4. Protein purification

Membrane solubilization was carried out by adding a 20%(*w*/*v*) solution of DDM to 150 ml resuspended membranes to give a final detergent concentration of 1.5%(*w*/*v*). The mixture was mixed at room temperature on a benchtop rocker, after which the mixture was spun at 4000*g* (20 min, 4°C) to remove any insoluble material. The solubilized membranes were incubated with 7 ml TALON cobalt metal-affinity resin (Takada) equilibrated with wash buffer [50 m*M* HEPES, 500 m*M* NaCl, 15%(*w*/*v*) glycerol, 50 m*M* imidazole, 2 m*M* *β*ME, 100 µ*M* PMSF pH 7.5] and 0.01%(*w*/*v*) DDM for 4 h at 4°C on a rocker. The TALON resin was then washed twice by the addition of 30 column volumes of wash buffer plus 0.01%(*w*/*v*) DDM (for each wash), followed by a low-speed centrifugation (700*g*, 5 min, 4°C) to separate the resin. The detergent DDM was exchanged with $C_{12}E_7$ by rinsing the TALON resin twice with 20 column volumes of wash buffer in the presence of 0.04%(*w*/*v*) $C_{12}E_7$.

ZMPSTE24 was eluted with five column volumes of elution buffer [50 m*M* HEPES, 150 m*M* NaCl, 15%(*w*/*v*) glycerol, 500 m*M* imidazole, 0.04%(*w*/*v*) $C_{12}E_7$, 2 m*M* *β*ME, 100 µ*M* PMSF pH 7.5]. The fractions were pooled and concentrated to ∼10 ml using an Amicon spin concentrator with 50 kDa molecular-weight cutoff (50 kDa MWCO; Millipore–Sigma). The sample was loaded onto a desalting column (HiPrep 26/10, GE Healthcare) and eluted with desalting buffer [50 m*M* HEPES, 150 m*M* NaCl, 15%(*w*/*v*) glycerol, 0.04%(*w*/*v*) $C_{12}E_7$, 2 m*M* *β*ME, 100 µ*M* PMSF pH 7.5]. The ZMPSTE24-containing fractions were pooled and the concentration of ZMPSTE24 was calculated by measurement of the $A_{280\ nm}$ using a molar extinction coefficient of 140 775 M^{-1} cm^{-1} as experimentally determined by quantitative amino-acid analysis (Molecular Structural Facility, UC-Davis Genome Center). The C-terminal polyhistidine tag was cleaved by the addition of 2.5 mg His_6-3C protease to 10 mg ZMPSTE24. The cleavage reaction was allowed to proceed overnight (12–15 h) at 4°C. The cleavage reaction was then incubated with 2.5 ml Ni–NTA agarose resin (Qiagen) for 90 min at 4°C on a rocker. The cleaved ZMPSTE24 sample was concentrated to ∼2 ml using an Amicon 50 kDa MWCO spin concentrator. After an additional centrifugation (17 000*g* for 10 min) of the retentate, it was loaded onto a preparative size-exclusion chromatography (SEC) column (Superdex 200, 10/60 column; GE Healthcare) equilibrated with SEC buffer [20 m*M* HEPES, 150 m*M* NaCl, 5%(*w*/*v*) glycerol, 0.04%(*w*/*v*) $C_{12}E_7$, 2 m*M* *β*ME pH 7.5]. The column was eluted with the same buffer at a flow rate of 0.7 ml min^{-1}. The ZMPSTE24-containing fractions were pooled, concentrated (using an Amicon 50 kDa MWCO spin concentrator) to between 8 and 10 mg ml^{-1} (corresponding to an approximately 30-fold reduction in volume from the original SEC fractions), snap-frozen in liquid nitrogen and stored at −80°C. A total of ∼3 mg of pure ZMPSTE24 was isolated from ∼160 g of yeast cells.

2.5. Enzyme-kinetics assay of ZMPSTE24

Steady-state enzyme kinetics of ZMPSTE24 were characterized using an intramolecular quenched-fluorescence (IQF) assay, with systematic errors arising from inner-filter and nonspecific quenching effects corrected as described in a previous methodological publication from our laboratory (Arachea & Wiener, 2017). The fluorogenic peptide substrate Abz-KSKTKSVIK-Dnp was prepared in 2.6%(*v*/*v*) DMSO and the molar concentration was determined by measurement of the absorbance at 360 nm using a molar extinction coefficient of ε = 17 530 M^{-1} cm^{-1} for ε-DNP-lysine (Ramachandran & Sastry, 1962). The enzyme reaction consisted of 0.65 mg ml^{-1} yeast membranes (containing overexpressed ZMPSTE24) in assay buffer (100 m*M* HEPES, 5 m*M* $MgCl_2$ pH 7.5) with variable peptide substrate concentrations (0–40 µ*M*) in a total sample volume of 200 µl. After 1 min equilibration, the reaction was monitored by following the increase in fluorescence for 3 min using a M5 SpectroMax plate reader (Molecular Devices) with excitation and emission wavelengths set to 320 and 420 nm, respectively. Initial velocity (V_i) values were determined from linear fits of the corrected fluorescence *versus* time data, and the kinetics parameters were determined by fitting the data to Michaelis–Menten kinetics with *GraphPad Prism* (GraphPad Software). All measurements were performed in triplicate.

2.6. Phosphoramidon inhibition

Neat DMSO was added to dissolve a freshly opened ampoule of lyophilized phosphoramidon, and its concentration was calculated from the mass reported by the manufacturer. Aliquots of ZMPSTE24 membranes (0.65 mg ml^{-1}) in assay buffer were incubated with various concentrations of phosphoramidon (0–100 µ*M*) for 10 min in the dark, after which the enzymatic reaction was initiated by the addition of 40 or 80 µ*M* fluorogenic peptide substrate. V_i values were used to calculate the percentage activities relative to the control (*i.e.* enzyme reaction without phosphoramidon). IC_{50} values

were calculated from activity (%) *versus* phosphoramidon concentration data using a four-parameter logistic (4PL) dose–response model (*GraphPad Prism*).

2.7. Crystallization of the phosphoramidon–ZMPSTE24 complex

Hanging-drop vapor diffusion was used for co-crystallization of the phosphoramidon–ZMPSTE24 complex; the method was modified from a recent crystallization report of ZMPSTE24 (Clark *et al.*, 2017). Prior to crystallization setups, 5.5 mg ml^{-1} (98.5 µ*M*) ZMPSTE24 was incubated with 845 µ*M* phosphoramidon (solubilized with 100% DMSO) for 1 h on ice. Protein stock solution was diluted with detergent-free buffer [20 m*M* HEPES, 150 m*M* NaCl, 5%(*w*/*v*) glycerol, 2 m*M* *β*ME pH 7.5] and the ZMPSTE24–phosphoramidon solution contained 5%(*v*/*v*) DMSO. Drops were formed from 1.33 µl protein solution and 0.67 µl reservoir solution [27% PEG 3350, 170 m*M* ammonium sulfate, 15%(*v*/*v*) glycerol, 50 m*M* HEPES pH 7.5] at room temperature (23°C) and then immediately transferred to 4°C for crystal growth. Needle-like crystals of 50–400 µm in size appeared 1–3 d after setup. Crystals were harvested 21 d after setup and plunge-cooled, without additional cryoprotection, in liquid nitrogen.

2.8. X-ray data collection

Data collection was performed on GM/CA CAT 23-ID-D at the Advanced Photon Source (APS), Argonne National Laboratory using a wavelength of 1.03 Å and a beam size of 10 µm. Raster scans were used first to identify single crystals and subsequently to identify the termini of the needle-like crystals to facilitate helical data collection across the entire crystal body. Diffraction data processing was performed with the GM/CA CAT 23-ID-D automated processing pipeline using the programs *XDS* (for indexing and integration) (Kabsch, 2010) followed by *POINTLESS* (for point-group determination) and *AIMLESS* (for merging and scaling) (Evans & Murshudov, 2013). Diffraction data were truncated to a maximum resolution of 3.85 Å based on a high-resolution shell $CC_{1/2}$ and $I/\sigma(I)$ of ~0.3 and 0.5, respectively (Karplus & Diederichs, 2015).

2.9. Structure determination and refinement

Phasing of the ZMPSTE24–phosphoramidon co-crystal structure was performed *via* molecular replacement using *Phaser* (McCoy *et al.*, 2007) from the *PHENIX* program suite (Adams *et al.*, 2010). Refinement was performed using *phenix.refine* (Afonine *et al.*, 2012), and model building and viewing utilized *Coot* (Emsley *et al.*, 2010). A sculpted, truncated search model consisting of a high-resolution ZMPSTE24 monomer (PDB entry 5syt; Clark *et al.*, 2017) was used as a search model; portions of the N- and C-termini (Δ10–15 and Δ471–480), as well as external loops (Δ284–292 and Δ311–322) and the transmembrane helix II (Δ61–99), were removed. Molecular replacement resulted in a robust solution (TFZ = 27.5) in space group $P2_1$, placing two copies in the asymmetric unit. Inspection of the initial maps after a single round of rigid-body refinement revealed that transmembrane helix II could be placed in only one of the two monomers in the asymmetric unit. Outside of this distinction, both monomers of the asymmetric unit were modeled identically using twofold NCS-averaged $2mF_o - F_c$ and $mF_o - F_c$ difference maps. Owing to the modest resolution (3.85 Å) of the diffraction data, neither real-space nor *xyz* reciprocal-space positional refinement was performed; only individual atomic displacement parameters (ADPs) were iteratively adjusted. The final structure of the ZMPSTE24–phosphoramidon complex has been deposited in the PDB with accession code 6bh8. Data-collection and refinement statistics are given in Table 1.

Table 1
Data-collection and refinement statistics.

Values in parentheses are for the outer shell.

Data collection	
Space group	$P2_1$
a, *b*, *c* (Å)	93.33, 84.66, 132.02
α, *β*, *γ* (°)	90, 96.26, 90
Wavelength (Å)	1.03
Resolution range (Å)	47.0–3.85 (3.99–3.85)
R_{meas}†	0.6127 (2.729)
$CC_{1/2}$	0.977 (0.326)
CC*	0.994 (0.701)
Multiplicity	3.2 (3.3)
$\langle I/\sigma(I)\rangle$‡	2.2 (0.54)
Completeness (%)	97.8 (97.4)
Refinement	
Resolution range (Å)	47.0–3.85 (3.95–3.85)
No. of reflections, working set	19241 (1230)
No. of reflections, test set	1909 (136)
R_{work}§/R_{free}¶ (%)	33.8/37.1
No. of atoms	
Protein	6383
Ion	2
Ligand	116
Average *B* factors (Å^2)	
Protein	132.2
Ion	171.8
Ligand	121.3
Ramachandran plot	
Most favored (%)	98
Allowed (%)	2
PDB code	6bh8

† $R_{meas} = \sum_{hkl}\{N(hkl)/[N(hkl)-1]\}^{1/2}\sum_i |I_i(hkl) - \langle I(hkl)\rangle|/\sum_{hkl}\sum_i I_i(hkl)$, where $I_i(hkl)$ is the observed intensity and $\langle I(hkl)\rangle$ is the average intensity of symmetry-related reflections. ‡ $\langle I/\sigma(I)\rangle$ is the ratio of the mean intensity to the mean standard deviation of intensity. § $R_{work} = \sum_{hkl}||F_{obs}| - |F_{calc}||/\sum_{hkl}|F_{obs}|$, where F_{obs} and F_{calc} are the observed and calculated structure factors, respectively. ¶ R_{free} was calculated using a randomly chosen 10% of the reflections.

3. Results and discussion

3.1. Phosphoramidon inhibition of ZMPSTE24

Isolated yeast membranes containing overexpressed ZMPSTE24 were tested for susceptibility to phosphoramidon inhibition against a soluble fluorogenic ZMPSTE24 substrate, Abz-KSKTKSVIK-Dnp. This substrate is derived from a previously designed prenylated substrate, Abz-KSKTKC(farnesyl)VIK-Dnp, originally derived from K-Ras for use in characterization of the CaaX protease Rce1p (Hollander *et al.*, 2000) and subsequently modified for increased selectivity for

ZMPSTE24 over Rce1p (Manandhar *et al.*, 2007). [We have previously used this prenylated substrate, Abz-KSKTKC(farnesyl)VIK-Dnp, extensively in studies of ZMPSTE24 and a yeast ortholog (Hildebrandt *et al.*, 2016; Arachea & Wiener, 2017)]. Proteolysis of this substrate obeys Michaelis–Menten kinetics, with K_m and V_{max} values of 10.0 ± 0.5 μ*M* and 0.82 ± 0.02 n*M* s^{-1}, respectively (Fig. 1*a*). Phosphoramidon displays competitive inhibition against soluble gluzincins and their respective substrates (Komiyama, Suda *et al.*, 1975; Kenny, 1977; Rose *et al.*, 2002). To test whether ZMPSTE24 was susceptible to phosphoramidon inhibition and to make a preliminary assignment of its mode of inhibition, IC_{50} measurements of phosphoramidon at two substrate concentrations, 40 μ*M* (Fig. 1*b*) and 80 μ*M* (Fig. 1*c*), were performed, yielding values of 7.6 ± 1.1 and 10.5 ± 1.2 μ*M*, respectively. This observed increase in IC_{50} (2.9 ± 1.6 μ*M*; *P* value < 0.1) with increasing substrate concentrations provides preliminary evidence consistent with competitive inhibition by phosphoramidon (Brooks *et al.*, 2004).

3.2. X-ray crystal structure of the phosphoramidon–ZMPSTE24 complex

Crystals of the phosphoramidon–ZMPSTE24 complex diffracted isotropically to a modest resolution (3.85 Å). Our ability to determine an accurate structure of the complex was enabled by the use of Pearson's correlation coefficient ($CC_{1/2}$) to evaluate the limits of usable (nonzero information content) diffraction data (Karplus & Diederichs, 2015). Use of $CC_{1/2}$ indicated clearly that the use of data to 3.85 Å resolution was fully warranted. [By comparison, the use of a previous 'popular' $\langle I/\sigma(I)\rangle$ < 2 cutoff would have yielded a data set to ∼6 Å resolution.] A feature of using this more objective and modern statistical approach to determine useful resolution is that for weakly diffracting crystals such as those of the phosphoramidon–ZMPSTE24 complex R_{meas} can appear anomalously (or even wrongly) large in magnitude. However, $CC_{1/2}$ analysis unambiguously indicates that such high R_{meas} values are fully compatible with low signal-to-noise data possessing nonzero information content.

Gluzincins, with the exception of the so-called 'mini-gluzincins' (López-Pelegrín *et al.*, 2013), contain an HE*xx*H . . . E motif centered around the zinc active-site center. The active-site residues of ZMPSTE24 are located at the base of the large, intramembrane cavern (Fig. 2*a*), where a pair of transmembrane helices provide the zinc-chelating residues (His335, His339 and Glu415) and the catalytic base (Glu336). Inspection of the active site of ZMPSTE24 revealed significant density for NCS-averaged $2mF_o - F_c$ and $mF_o - F_c$ difference maps with an asymmetric molecular envelope, as expected for phosphoramidon (Fig. 2*b*). Large peaks of positive difference density indicated the position of the electron-dense indole ring and phosphoramidate moiety coordinating the Zn atom. Additionally, a region of significant electron density above the phosphoramidate/zinc center was consistent with placement of

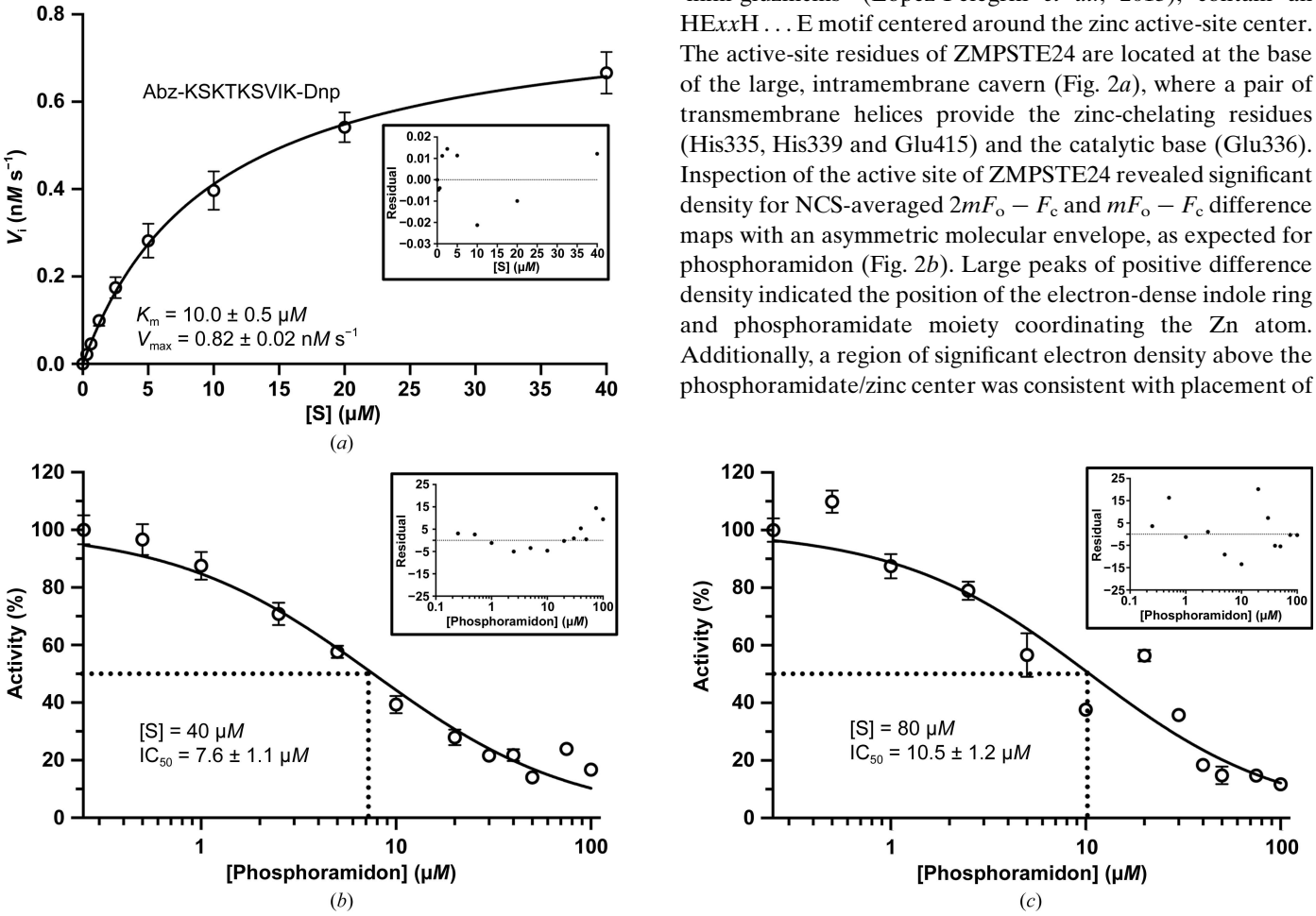

Figure 1
Inhibition of ZMPSTE24 membranes by phosphoramidon. The boxed insets display residual plots for each fit of the data to the model. (*a*) Activity of ZMPSTE24 against the fluorogenic peptide substrate Abz-KSKTKSVIK-Dnp. Initial velocity (V_i) data (triplicate; mean ± standard error of the mean) *versus* substrate concentration [S] were fitted to a Michaelis–Menten steady-state kinetics model (R^2 = 0.999). (*b*) Dose–response curve of phosphoramidon at 40 μ*M* peptide substrate (R^2 = 0.992) and (*c*) dose–response curve of phosphoramidon at 80 μ*M* peptide substrate (R^2 = 0.922). The increase in IC_{50} as a function of substrate concentration provides preliminary evidence consistent with competitive inhibition (Brooks *et al.*, 2004). Competitive inhibition by phosphoramidon is observed for the gluzincins neprilysin (Kenny, 1977) and thermolysin (Komiyama, Suda *et al.*, 1975).

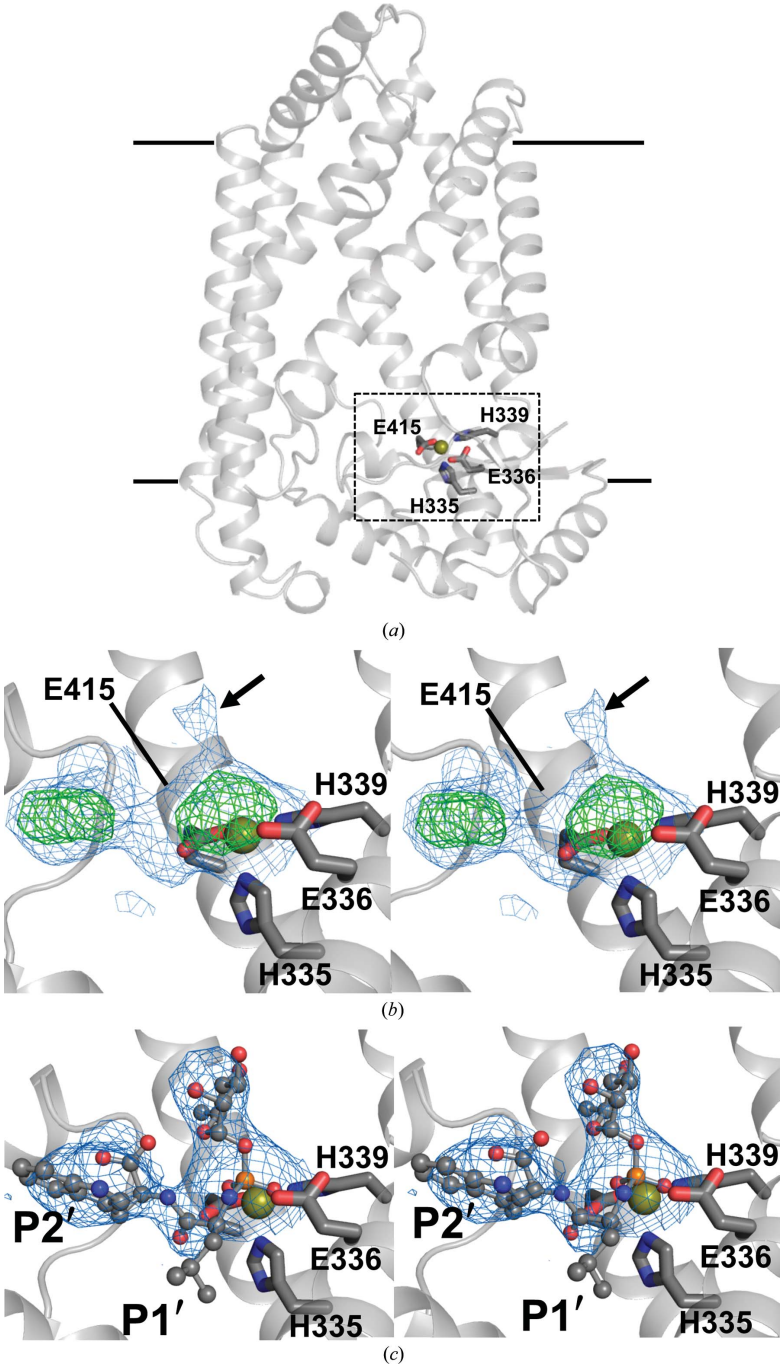

Figure 2
Crystallographic structure determination of the ZMPSTE24–phosphoramidon complex. (*a*) Ribbon diagram of the ZMPSTE24 monomer highlighting the position of the zinc center (gold sphere) and the canonical gluzincin HE*xx*H . . . E motif (gray sticks). ZMPSTE24 residues His335, His339 and Glu415 are zinc ligands, while Glu336 acts as the catalytic base. Black lines indicate the approximate membrane boundaries. The dashed box indicates the cutaway view used in (*b*) and (*c*). (*b*) The twofold NCS-averaged $2mF_o - F_c$ maps (blue mesh contoured at 1.5σ) and positive $mF_o - F_c$ difference map peaks (green mesh contoured at 4.5σ) reveal a molecular envelope consistent with the location of phosphoramidon near the zinc center and the HE*xx*H . . . E motif. The arrow indicates the putative position of the rhamnose ring of phosphoramidon. (*c*) The final modeled and refined phosphoramidon molecule (shown in ball-and-stick representation) with overlapping, refined $2mF_o - F_c$ maps (blue mesh contoured at 1.5σ) coordinating the zinc center of ZMPSTE24. The phosphorus atom of the phosphoramidon molecule is colored orange. The phophoramidon specificity pocket-binding moieties tryptophan (P2′) and leucine (P1′) are explicitly labeled for clarity.

the rhamnose group. The phosphoramidon molecule refines reasonably at 100% occupancy, with *B* factors similar to those of the surrounding protein residues and the zinc centre (100–150 Å^2; Fig. 2*c*). The phosphoramidon tryptophan (P2′) and leucine (P1′) moieties bind in a canonical fashion to other structurally determined gluzincins (see below).

3.3. Relation between phosphoramidon binding to ZMPSTE24 and to soluble gluzincins

The active-site residues of all protease enzymes belong to one of two interdependent functional classes that facilitate peptide cleavage: (i) residues interfacing with peptide backbone atoms and/or promoting cleavage of the scissile bond (*i.e.* catalytic residues) or (ii) residues responsible for recognizing specific peptide side-chain identities or chemical properties (*i.e.* specificity-pocket residues). Each element of the active-site structure works in concert to position the appropriate scissile peptide bond, which in the case of zinc metalloproteases is in proximity to the zinc center (Schechter & Berger, 1967, 1968). While the natural product inhibitor phosphoramidon exploits both of these functional classes of active-site protease residues, it primarily targets specificity pockets that are present in gluzincins, as manifested by the ability of phosphoramidon to inhibit both thermolysin and neprilysin (Suda *et al.*, 1973; Rose *et al.*, 2002). However, the extent to which catalytic and specificity-pocket residues of gluzincins are maintained within the cavernous reaction cavity of the integral membrane protein gluzincin ZMPSTE24 had yet to be investigated, in detail, prior to this present study.

Comparison of the structure of ZMPSTE24 complexed with phosphoramidon with the known structures of the phosphoramidon–thermolysin (Tronrud *et al.*, 1986) and phosphoramidon–neprilysin (Oefner *et al.*, 2000) complexes reveals conservation of both the catalytic and specificity-pocket regions (Fig. 3). Catalytic residues 'sandwiching' the phosphoramidon molecule are generally conserved among the three gluzincins (Figs. 3*a*, 3*b* and 3*c*) including, using ZMPSTE24 numbering, the β-strand-derived Asn265 side-chain amide and Ala266 main-chain carbonyl as well as an opposing α-helical element providing the His459 and Arg465 side chains. The notable exception is the presence of a tyrosine residue (Tyr157; Fig. 3*b*) in thermolysin that forms an extra hydrogen-bond interaction with the rhamnose ring of phosphoramidon. The specificity pockets of gluzincins are positioned to bind residues immediately C-terminal to the scissile bond (S1′) and C-terminally distal to the scissile bond (S2′) (Figs. 3*d*, 3*e* and 3*f*), thereby interacting with the leucine (P1′) and tryptophan (P2′) of

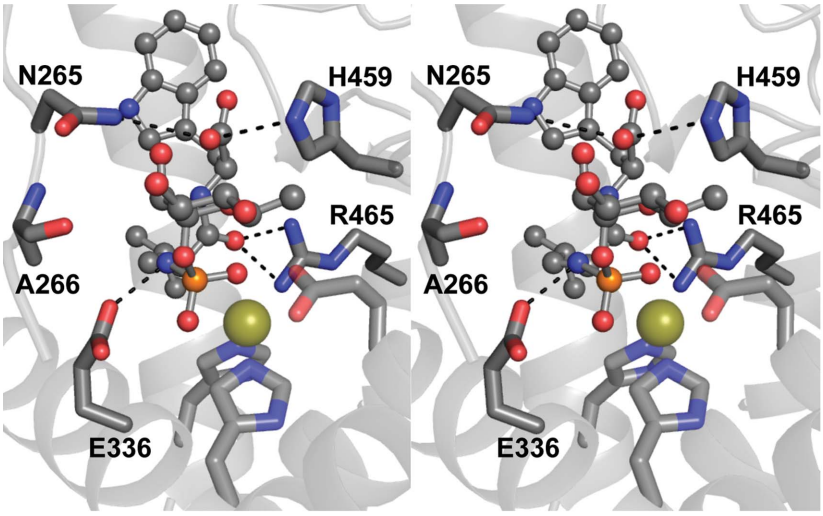

(*a*)

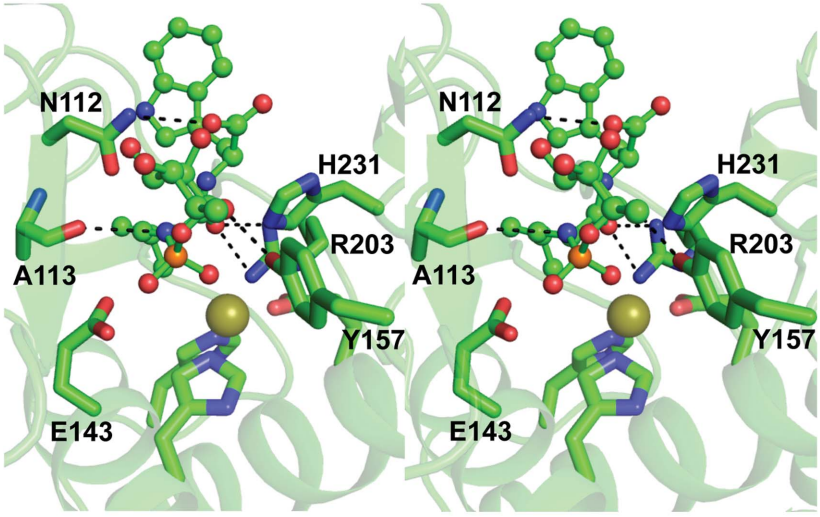

(*b*)

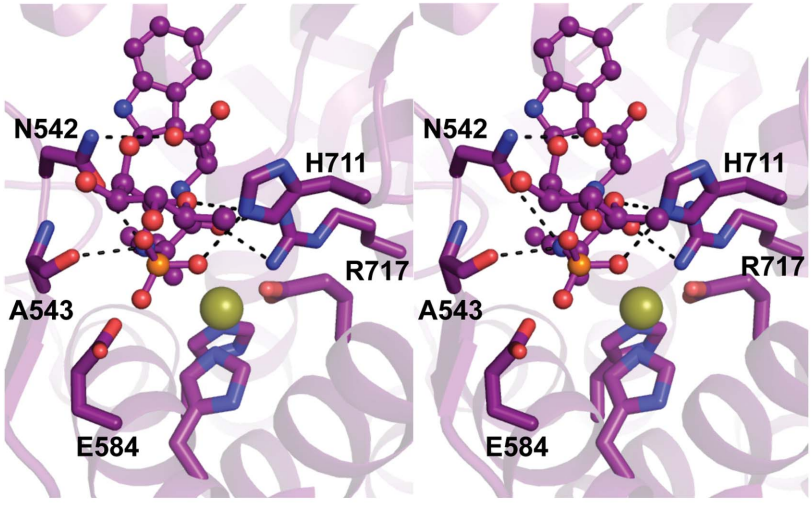

(*c*)

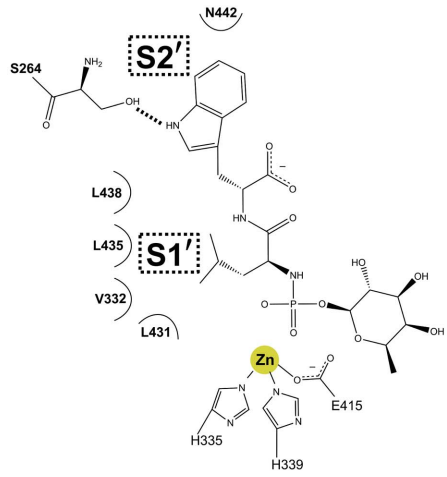

(*d*)

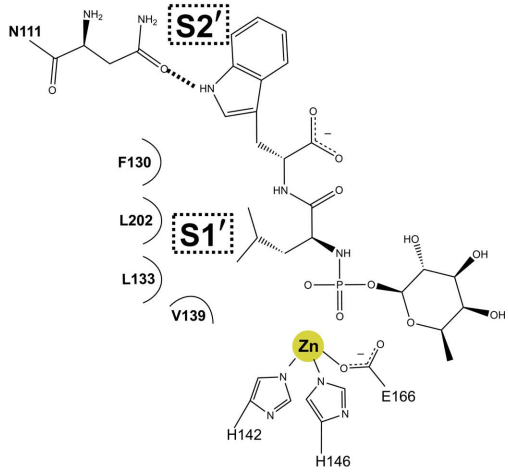

(*e*)

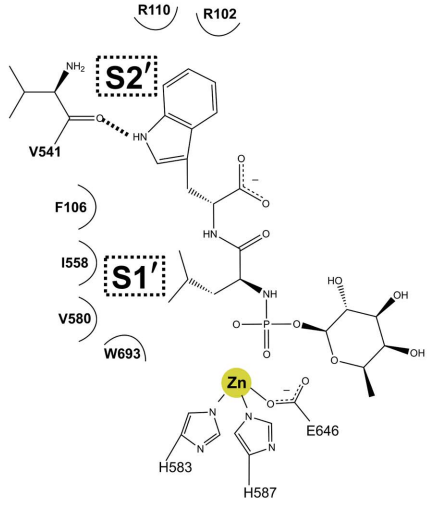

(*f*)

Figure 3
The phosphoramidon-binding specificity pocket of ZMPSTE24 compared with those of the gluzincins thermolysin and neprilysin. The left-hand panel illustrates the residues beyond the conserved HE*xx*H . . . E motif that form hydrogen-bond contacts with phosphoramidon in (*a*) ZMPSTE24 (PDB entry 6bh8; this work), (*b*) thermolysin (PDB entry 1tlp; Tronrud *et al.*, 1986) and (*c*) neprilysin (PDB entry 1dmt; Oefner *et al.*, 2000). The right-hand panel indicates the residues responsible for forming the specificity pockets for residues immediately C-terminal to the scissile bond (S1′) and C-terminally distal to the scissile bond (S2′) as present in (*d*) ZMPSTE24, (*e*) thermolysin and (*f*) neprilysin. Note that the specificity pockets lie below the plane of the zinc center and catalytic residues depicted in (*a*), (*b*) and (*c*).

phosphoramidon (Fig. 2*c*). In addition to their conserved consensus motif and zinc-ligation scheme, gluzincins share a preference for aliphatic or aromatic residues at the substrate (P1′): a structural motif exploited by phosphoramidon, resulting in its enhanced affinity towards gluzincins (Komiyama, Aoyagi *et al.*, 1975; Salvesen & Narbonne, 2001). Indeed, comparison of the S1′ specificity pocket of ZMPSTE24 with those of thermolysin and neprilysin reveals a similar hydrophobic pocket, with the exception of the aromatic phenylalanine that is present in thermolysin (Phe130) and neprilysin (Phe106) but is substituted by a leucine (Leu438) in ZMPSTE24. The indole ring of the P2′ tryptophan in phosphoramidon makes limited nonbonded contacts with the S2′ specificity pockets compared with the extensive additional interactions of neprilysin with a pair of arginine residues (Arg118 and Arg102; Fig. 3*f*). Overall, the differential constitution of the ZMPSTE24 specificity pocket, as opposed to those of thermolysin and neprilysin, suggests that the potency of phosphoramidon is significantly diminished in ZMPSTE24 compared with thermolysin and neprilysin.

4. Conclusions

Functional and structural characterization of the interaction of the zinc metalloprotease natural product peptidic inhibitor phosphoramidon with ZMPSTE24 indicates that its mechanism of action on this integral membrane protein zinc metalloprotease is likely to be similar to its action upon soluble gluzincins (*i.e.* competitive inhibition), but needs to be confirmed by more rigorous and comprehensive titrations of phosphoramidon against a larger subset of the substrate concentrations used in our steady-state kinetic assays. The structural binding mode of phosphoramidon to ZMPSTE24 is similar to that observed in soluble gluzincins, but we predict lessened potency. This prediction can be rationalized by an observation of less extensive interactions of the inhibitor with the S1′ and S2′ specificity pockets of ZMPSTE24 compared with the soluble gluzincins. Therefore, despite the provocatively novel structural aspects of ZMPSTE24, namely the presence of a 14 000 Å^3 intramembranous reaction cavity in which the active site is sequestered away from bulk solvent, ZMPSTE24 shares significant structural and functional properties with soluble gluzincins.

Acknowledgements

We would like to thank Dr Michael Becker and colleagues at GM/CA-CAT for technical support during data collection. We would also like to thank the reviewers of this manuscript for perceptive comments, critique and suggestions, particularly regarding the treatment and reporting of our enzymological data.

Funding information

GM/CA@APS has been funded in whole or in part with Federal funds from the National Cancer Institute (ACB-12002) and the National Institute of General Medical Sciences (AGM-12006). This research used resources of the Advanced Photon Source, a US Department of Energy (DOE) Office of Science User Facility operated for the DOE Office of Science by Argonne National Laboratory under Contract No. DE-AC02-06CH11357. This work was supported by National Institutes of Health Grant R01GM108612.

References

Adams, P. D. *et al.* (2010). *Acta Cryst.* D**66**, 213–221.
Afonine, P. V., Grosse-Kunstleve, R. W., Echols, N., Headd, J. J., Moriarty, N. W., Mustyakimov, M., Terwilliger, T. C., Urzhumtsev, A., Zwart, P. H. & Adams, P. D. (2012). *Acta Cryst.* D**68**, 352–367.
Arachea, B. T. & Wiener, M. C. (2017). *Anal. Biochem.* **522**, 30–36.
Ast, T., Michaelis, S. & Schuldiner, M. (2016). *Cell*, **164**, 103–114.
Barrowman, J., Hamblet, C., George, C. M. & Michaelis, S. (2008). *Mol. Biol. Cell*, **19**, 5398–5408.
Barrowman, J., Wiley, P. A., Hudon-Miller, S. E., Hrycyna, C. A. & Michaelis, S. (2012). *Hum. Mol. Genet.* **21**, 4084–4093.
Boyartchuk, V. L., Ashby, M. N. & Rine, J. (1997). *Science*, **275**, 1796–1800.
Brooks, H. B., Geeganage, S., Kahl, S. D., Montrose, C., Sittampalam, S., Smith, M. C. & Weidner, J. R. (2004). *Assay Guidance Manual*, edited by G. S. Sittampalam *et al.* Bethesda: Eli Lilly & Company and the National Center for Advancing Translational Sciences.
Clark, K. M., Fedoriw, N., Robinson, K., Connelly, S. M., Randles, J., Malkowski, M. G., DeTitta, G. T. & Dumont, M. E. (2010). *Protein Expr. Purif.* **71**, 207–223.
Clark, K. M., Jenkins, J. L., Fedoriw, N. & Dumont, M. E. (2017). *Protein Sci.* **26**, 242–257.
Coffinier, C., Hudon, S. E., Farber, E. A., Chang, S. Y., Hrycyna, C. A., Young, S. G. & Fong, L. G. (2007). *Proc. Natl Acad. Sci. USA*, **104**, 13432–13437.
Dittmer, T. A. & Misteli, T. (2011). *Genome Biol.* **12**, 222.
Emsley, P., Lohkamp, B., Scott, W. G. & Cowtan, K. (2010). *Acta Cryst.* D**66**, 486–501.
Evans, P. R. & Murshudov, G. N. (2013). *Acta Cryst.* D**69**, 1204–1214.
Fujimura-Kamada, K., Nouvet, F. J. & Michaelis, S. (1997). *J. Cell Biol.* **136**, 271–285.
Goulbourne, C. N. & Vaux, D. J. (2010). *Biochem. Soc. Trans.* **38**, 292–296.
Hildebrandt, E. R., Arachea, B. T., Wiener, M. C. & Schmidt, W. K. (2016). *J. Biol. Chem.* **291**, 14185–14198.
Hollander, I., Frommer, E. & Mallon, R. (2000). *Anal. Biochem.* **286**, 129–137.
Hooper, N. M. (1994). *FEBS Lett.* **354**, 1–6.
Ito, H., Fukuda, Y., Murata, K. & Kimura, A. (1983). *J. Bacteriol.* **153**, 163–168.
Jones, E. W. (1991). *Methods Enzymol.* **194**, 428–453.
Jonikas, M. C., Collins, S. R., Denic, V., Oh, E., Quan, E. M., Schmid, V., Weibezahn, J., Schwappach, B., Walter, P., Weissman, J. S. & Schuldiner, M. (2009). *Science*, **323**, 1693–1697.
Kabsch, W. (2010). *Acta Cryst.* D**66**, 125–132.
Karplus, P. A. & Diederichs, K. (2015). *Curr. Opin. Struct. Biol.* **34**, 60–68.
Kayatekin, C., Amasino, A., Gaglia, G., Flannick, J., Bonner, J. M., Fanning, S., Narayan, P., Barrasa, M. I., Pincus, D., Landgraf, D., Nelson, J., Hesse, W. R., Costanzo, M., AMP T2D-GENES Consortium, Myers, C. L., Boone, C., Florez, J. C. & Lindquist, S. (2018). *Cell*, **173**, 62–73.
Kenny, A. J. (1977). *Ciba Found. Symp.*, pp. 209–215.
Komiyama, T., Aoyagi, T., Takeuchi, T. & Umezawa, H. (1975). *Biochem. Biophys. Res. Commun.* **65**, 352–357.

Komiyama, T., Suda, H., Aoyagi, T., Takeuchi, T., Umezawa, H., Fujimoto, K. & Umezawa, S. (1975). *Arch. Biochem. Biophys.* **171**, 727–731.
López-Pelegrín, M., Cerdà-Costa, N., Martínez-Jiménez, F., Cintas-Pedrola, A., Canals, A., Peinado, J. R., Marti-Renom, M. A., López-Otín, C., Arolas, J. L. & Gomis-Rüth, F. X. (2013). *J. Biol. Chem.* **288**, 21279–21294.
Manandhar, S. P., Hildebrandt, E. R. & Schmidt, W. K. (2007). *J. Biomol. Screen.* **12**, 983–993.
McCoy, A. J., Grosse-Kunstleve, R. W., Adams, P. D., Winn, M. D., Storoni, L. C. & Read, R. J. (2007). *J. Appl. Cryst.* **40**, 658–674.
Meissner, D., Odman-Naresh, J., Vogelpohl, I. & Merzendorfer, H. (2010). *Mol. Biol. Cell*, **21**, 2425–2433.
Oefner, C., D'Arcy, A., Hennig, M., Winkler, F. K. & Dale, G. E. (2000). *J. Mol. Biol.* **296**, 341–349.
Ordóñez, G. R., Puente, X. S., Quesada, V. & López-Otín, C. (2009). *Methods Mol. Biol.* **539**, 33–47.
Pryor, E. E. Jr, Horanyi, P. S., Clark, K. M., Fedoriw, N., Connelly, S. M., Koszelak-Rosenblum, M., Zhu, G., Malkowski, M. G., Wiener, M. C. & Dumont, M. E. (2013). *Science*, **339**, 1600–1604.
Quigley, A., Dong, Y. Y., Pike, A. C. W., Dong, L., Shrestha, L., Berridge, G., Stansfeld, P. J., Sansom, M. S. P., Edwards, A. M., Bountra, C., von Delft, F., Bullock, A. N., Burgess-Brown, N. A. & Carpenter, E. P. (2013). *Science*, **339**, 1604–1607.
Ragnauth, C. D., Warren, D. T., Liu, Y., McNair, R., Tajsic, T., Figg, N., Shroff, R., Skepper, J. & Shanahan, C. M. (2010). *Circulation*, **121**, 2200–2210.
Ramachandran, L. K. & Sastry, L. V. (1962). *Biochemistry*, **1**, 75–78.
Rose, C., Voisin, S., Gros, C., Schwartz, J. C. & Ouimet, T. (2002). *Biochem. J.* **363**, 697–705.
Salvesen, G. S. & Narbonne, H. (2001). *Proteolytic Enzymes: A Practical Approach*, 2nd ed., edited by J. S. Bond & R. J. Beynon, pp. 105–130. Oxford University Press.
Schechter, I. & Berger, A. (1967). *Biochem. Biophys. Res. Commun.* **27**, 157–162.
Schechter, I. & Berger, A. (1968). *Biochem. Biophys. Res. Commun.* **32**, 898–902.
Suda, H., Aoyagi, T., Takeuchi, T. & Umezawa, H. (1973). *J. Antibiot.* **26**, 621–623.
Tipper, D. J. & Harley, C. A. (2002). *Mol. Biol. Cell*, **13**, 1158–1174.
Tronrud, D. E., Monzingo, A. F. & Matthews, B. W. (1986). *Eur. J. Biochem.* **157**, 261–268.
Worman, H. J. (2012). *J. Pathol.* **226**, 316–325.